J|A|C|S
ARTICLES
Published on Web 02/11/2004

Simulations of the Large Kinetic Isotope Effect and the Temperature Dependence of the Hydrogen Atom Transfer in Lipoxygenase

Mats H. M. Olsson,* Per E. M. Siegbahn,† and Arieh Warshel*

Contribution from the Chemistry Department, University of Southern California, Los Angeles, California 90089-1062, and Stockholm University, Department of Physics, ALBANOVA, S106 91 Stockholm, Sweden

Received July 11, 2003; E-mail: molsson@usc.edu; warshel@usc.edu

Abstract: Elucidating the role of nuclear quantum mechanical (NQM) effects in enzyme catalysis is a topic of significant current interest. Despite the great experimental progress in this field it is important to have theoretical approaches capable of evaluating and analyzing nuclear quantum mechanical contributions to catalysis. In this study, we use the catalytic reaction of lipoxygenase, which is characterized by an extremely large kinetic isotope effect, as a challenging test case for our simulation approach. This is done by applying the quantum classical path (QCP) method with an empirical valence bond potential energy surface. Our computational strategy evaluates the relevant NQM corrections and reproduces the large observed kinetic isotope effect and the temperature dependence of the H atom transfer reaction while being less successful with the D atom transfer reaction. However, the main point of our study is not so much to explore the temperature dependence of the isotope effect but rather to develop and validate an approach for calculations of nuclear quantum mechanical contributions to activation free energies. Here, we find that the deviation between the calculated and observed activation free energies is small for both H and D at all investigated temperatures. The present study also explores the nature of the reorganization energy in the enzyme and solution reactions. It is found that the outer-sphere reorganization energy is extremely small. This reflects the fact that the considered reaction involves a very small charge transfer. The implication of this finding is discussed in the framework of the qualitative vibronic model. The main point of the present study is, however, that the rigorous QCP approach provides a reliable computational tool for evaluating NQM contributions to catalysis even when the given reaction includes large tunneling contributions. Interestingly, our results indicate that the NQM effects in the lipoxygenase reaction are similar in the enzyme and in the reference solution reactions, and thus do not contribute to catalysis. We also reached similar conclusions in studies of other enzymes.

I. Introduction

In numerous enzymatic reactions one of the key steps, which is often also the rate-limiting step, is a transfer of protons or hydrogen atoms. Since these are comparatively light particles, the transfer is often associated with significant nuclear quantum mechanical (NQM) effects (e.g. zero-point energy and tunneling corrections). Thus, it is of significant interest to understand the magnitude of NQM effects in enzyme reactions and their possible contribution to enzyme catalysis.[1−8] In general, it is difficult to deduce the actual role of NQM effects in enzyme catalysis from current experimental approaches since it requires a comparison of the NQM contributions in the given enzymatic reaction with those of the same reaction in an uncatalyzed reference reaction, i.e., water solution[6] (for NQM effects to assist in catalysis, it should reduce the reaction barrier in the protein more than in the reference reaction). In some cases, such as enzymes utilizing metal centers, it might be very difficult to construct the relevant model system to study this reference reaction, which makes this comparison impossible. In other cases, the enzyme and solution reactions are different, in which the catalysis includes both the effect of changing the reaction mechanism from the one in water to that in the enzyme and the effect of changing the active-site environment from water solution to that of the protein. Finally, a complete analysis should also address the actual contributions of the protein that are supposedly responsible for enhancing the tunneling effect, and this information can usually not be obtained directly from experiments. Thus, it is important to augment the experimental information about kinetic isotope effects (KIE) by simulation approaches that are capable of reproducing the observed effects

† Stockholm University.

(1) Knapp, M. J.; Rickert, K.; Klinman, J. P. *J. Am. Chem. Soc.* **2002**, *124*, 3865−3874.
(2) Kemsley, J. *Chem. Eng. News* **2003**, *81*, 29−30.
(3) Doll, K. M.; Bender, B. R.; Finke, R. G. *J. Am. Chem. Soc.* **2003**, *125*, 10877−10884.
(4) Wang, S. X.; Mure, M.; Medzihradszky, K. F.; Burlingame, A. L.; Brown, D. E.; Dooley, D. M.; Smith, A. J.; Kagan, H. M.; Klinman, J. P. *Science* **1996**, *273*, 1078−1084.
(5) Lehnert, N.; Solomon, E. I. *J. Biol. Inorg. Chem.* **2003**, *8*, 294−305.
(6) Hwang, J. K.; Warshel, A. *J. Am. Chem. Soc.* **1996**, *118*, 11745−11751.
(7) Billeter, S. R.; Webb, S. P.; Agarwal, P. K.; Iordanov, T.; Hammes-Schiffer, S. *J. Am. Chem. Soc.* **2001**, *123*, 11262−11272.
(8) Hwang, J. K.; Warshel, A. *J. Phys. Chem.* **1993**, *97*, 10053−10058.

 10.1021/ja037233l CCC: $27.50

and then to evaluate the role of the protein or the solution environment in modulating these effects. In doing so, we must focus on the quantum mechanical correction to the activation free energy since this is the primary factor that determines the reaction rate (see below) and, thus, the possible catalytic effect.

The development of methods for simulating NQM effects in enzymatic reactions dates back to the early 1990s (see, e.g., refs 8, 9) and has recently been quite an active field.[6,7,10,11] However, most of the reactions studied this far involve relatively small NQM effects with KIE in the range of 2−10. Exploring systems with very large KIE may therefore provide a more stringent test on the available simulation methods and a clearer benchmark for assessing the role of NQM effects in enzyme catalysis. In the present study, we consider one of the most spectacular examples of NQM effects in enzyme catalysis as a benchmark, namely the reaction of lipoxygenase, which is a family of enzymes that dioxygenates polyunsaturated fatty acids.[12,13] Here, we report a microscopic simulation of the large kinetic isotope effect in soybean lipoxygenase (SLO-1) and its temperature dependence. This is, to the best of our knowledge, the first time that a very large nuclear quantum effect has been simulated in a protein while considering the full dynamics of the protein+solvent system. The basic reaction catalyzed by lipoxygenase enzymes is the peroxidation of 1,4-pentadiene containing fatty acids. This reaction is believed to proceed via a radical mechanism (although other suggestions have been proposed, it seems that the radical mechanism is presently the most widely supported[1,5,14]) where the initial and rate-limiting step consists of a hydrogen atom abstraction from the substrate to a non-heme iron active site. This transfer is associated with an exceptionally large kinetic isotope effect, $k_H/k_D \approx 80$,[1] which is significantly larger than what is commonly seen in proteins, $k_H/k_D \approx 3-8$. In a second step, the intermediate radical is oxygenated with molecular oxygen.

From a theoretical point of view, it is undoubtedly a challenge to try to account for the observed isotope effect in the protein by microscopic simulations without adjustable parameters. In previous studies,[1,5] the large kinetic isotope effect has been accounted for by fitting to the three-parameter vibronic formulation[15−17] (see also section II.3). Such a phenomenological fitting is rather straightforward but involves the following problems: First, it is not clear how the obtained macroscopic parameters relate to the corresponding microscopic system (see below). Second, the expression used in the phenomenological fitting is based on a treatment[16] that considers the system in the diabatic limit (small electronic overlap between the donor and acceptor) and evaluates the transition probability between the relevant vibronic states. Such an expression provides an excellent description of NQM corrections on electron-transfer reactions (see, e.g., refs 18−22) but might well be invalid in cases of proton and hydrogen atom transfer reactions where the electronic coupling is usually large and the system cannot be described by the Landau−Zener approximation. In other words, in such cases, the diabatic approximation might be invalid, and one should move to the adiabatic limit, which cannot be described by the simple vibronic formula (see Discussion in ref 16). Using the phenomenological vibronic formula, the observed experimental isotope effect can easily be reproduced even though the parameters (e.g., the reorganization energy and the electronic coupling) may not describe the actual physics of the given biological system. In this study, on the other hand, we present a fully microscopic simulation approach that considers explicitly the nuclear quantum mechanical effects in the substrate and protein+solvent system. Our approach is based on the quantum classical path (QCP) version[6,8] of the centroid path integral approach,[23−25] and on a DFT based empirical valence bond (EVB) potential energy surface. Using this approach, we have succeeded to reproduce the very large observed KIE based on an actual microscopic simulation approach rather than on a phenomenological model. This provides us with an approach that is capable of examining the effects of the protein on the overall NQM effects and, thus, its role in enzyme catalysis.

II. Methods

II.1. The EVB surface. To simulate chemical reactions in proteins, it is essential to have a reasonable potential energy surface. In the case of NQM calculations, which require long simulations to converge the free energy, it is also helpful if the relevant potential energy surface is available in an analytical form. In this respect the EVB approach provide a very powerful tool. The EVB method has been described extensively elsewhere (e.g., refs 26−29) and we only give a few key points here.

The EVB method is a QM/MM method that describes reactions by mixing resonance states (or more precisely diabatic states) that correspond to classical valence-bond (VB) structures, which represent the reactant intermediate (or intermediates) and product states. The potential energies of these diabatic states are represented by classical MM force fields of the form:

$$H_{ii} = \epsilon_i = \alpha^i_{gas} + U^i_{intra}(\mathbf{R},\mathbf{Q}) + U^i_{Ss}(\mathbf{R},\mathbf{Q},\mathbf{r},\mathbf{q}) + U_{ss}(\mathbf{r},\mathbf{q}) \quad (1)$$

Here, $\boldsymbol{R}$ and $\boldsymbol{Q}$ represent the atomic coordinates and charges of the diabatic states, and $\boldsymbol{r}$ and $\boldsymbol{q}$ are those of the surrounding protein and solvent. α^i_{gas} is the gas-phase energy of the ith diabatic state (where all the fragments are taken to be at infinity), $U_{intra}(\boldsymbol{R,Q})$ is the intramolecular potential of the solute system (relative to its minimum), $U_{Ss}(\boldsymbol{R,Q,r,q})$ represents the interaction between the solute (S) atoms and the surrounding (s) solvent and protein atoms. $U_{ss}(\boldsymbol{r,q})$ represents the potential energy of the protein/solvent system ("ss" designates surrounding−surrounding). ϵ_i is given by eq 1 from the diagonal elements of the EVB Hamiltonian (H_{EVB}). The off-diagonal elements of this Hamiltonian, H_{ij}, are assumed to be constant or they can be represented by a simple function such as an exponential function of the distances between the reacting atoms. These H_{ij} elements are assumed to be the same in the gas phase, in solutions and in the proteins. The adiabatic ground-state energy E_g and the corresponding eigenvector C_g are obtained by solving the secular equation.

(9) Hwang, J. K.; Chu, Z. T.; Yadav, A.; Warshel, A. *J. Phys. Chem.* **1991**, *95*, 8445−8448.
(10) Villà, J.; Warshel, A. *J. Phys. Chem. B* **2001**, *105*, 7887−7907.
(11) Gao, J. L.; Truhlar, D. G. *Ann. Rev. Phys. Chem.* **2002**, *53*, 467−505.
(12) Brash, A. R. *J. Biol. Chem.* **1999**, *274*, 23679−23682.
(13) Nelson, M. J.; Seitz, S. P. *Curr. Opin. Struct. Biol.* **1994**, *4*, 878−884.
(14) Borowski, T.; Broclawik, E. *J. Phys. Chem. B* **2003**, *107*, 4639−4646.
(15) Kuznetsov, A. M.; Ulstrup, J. *Can. J.Chem.* **1999**, *77*, 1085−1096.
(16) Warshel, A.; Chu, Z. T. *J. Chem. Phys.* **1990**, *93*, 4003−4015.
(17) German, E. D.; Kuznetsov, A. M. *J. Chem. Soc., Faraday Trans. I* **1981**, *77*, 397−412.
(18) Warshel, A.; Hwang, J. K. *J. Chem. Phys.* **1986**, *84*, 4938−4957.
(19) Levich, V. G. *Adv. Electrochem. Electrochem. Eng.* **1966**, 249−371.
(20) Kestner, N. R.; Logan, J.; Jortner, J. *J. Phys. Chem.* **1974**, *78*, 2148−2166.
(21) Efrima, S.; Bixon, M. *Chem. Phys.* **1976**, *13*, 447−460.
(22) Warshel, A. *Proc. Natl. Acad. Sci. U.S.A.* **1980**, *77*, 3105−3109.
(23) Gillan, M. J. *J. Phys. C: Solid State Phys.* **1987**, *20*, 3621−3641.
(24) Voth, G. A. *Adv. Chem. Phys.* **1996**, *93*, 135−218.
(25) Voth, G. A.; Chandler, D.; Miller, W. H. *J. Chem. Phys.* **1989**, *91*, 7749−7760.
(26) Chu, T. Z.; Villà, J.; Strajbl, M.; Schutz, C.; Shurki, A.; Warshel, A.; *Molaris*, beta 9.05, 2002.

$$H_{\mathbf{EVB}}C_{\mathbf{g}} = E_{\mathbf{g}}C_{\mathbf{g}} \quad (2)$$

The EVB treatment provides a natural picture of intersecting electronic states, which is useful for exploring environmental effects on chemical reactions in condensed phases.[27] The ground-state charge distribution of the reacting species ("solute") polarizes the surroundings ("solvent"), and the charges of each resonance structure of the solute then interacts with the polarized solvent.[27] This coupling enables the EVB model to capture the effect of the solvent on the quantum mechanical mixing of the different states of the solute. For example, in cases where ionic and covalent states are describing the solute, the solvent stabilizes the ionic state to a greater extent, and the resulting ground state has more ionic character and more solvation energy.

The simplicity of the EVB formulation makes it easy to obtain its analytical derivatives (using the Hellmann−Feynman theorem for eq 2) and, thus, to sample the EVB energy surface by MD simulations. Running such MD trajectories on the EVB surface of the reactant state can provide the free-energy function Δg that is needed to calculate the activation energy $\Delta g^{\ddagger}$. However, since trajectories on the reactant surface will reach the transition state only rarely, it is usually necessary to run a series of trajectories on potential surfaces that gradually drive the system from the reactant to the product state.[27] The EVB approach accomplishes this by changing the system adiabatically from one diabatic state to another. In the simple case of two diabatic states, this "mapping" potential, ϵ_m, can be written as a linear combination of the reactant and product potentials, ϵ_1 and ϵ_2:

$$\epsilon_m = (1 - \theta_m)\,\epsilon_1 + \theta_m\epsilon_2 \quad (0 \le \theta_m \le 1) \quad (3)$$

When θ_m is changed from 0 to 1 in n+1 fixed increments (θ_m = 0/n, 1/n, 2/n, ..., n/n), potentials with one or more of the intermediate values of θ_m will force the system to fluctuate near the TS.

The free energy ΔG_m associated with changing θ_m from 0 to m/n is evaluated by the FEP procedure described elsewhere. The free-energy functional that corresponds to the adiabatic ground-state surface E_g (in eq 2) is then obtained by the FEP-umbrella sampling (FEP/US) method,[29] which can be written as

$$\Delta g(x') = \Delta G_m - \beta^{-1}\ln\langle\delta(x - x')\exp[-\beta(E_g(x) - \epsilon_m(x))]\rangle_{\epsilon_m} \quad (4)$$

where ϵ_m is the mapping potential that keeps x in the region of x'. If the changes in ϵ_m are sufficiently gradual, the free-energy functional $\Delta g(x')$ obtained with several values of m overlap over a range of x', and patching together the full set of $\Delta g(x')$ gives the complete free-energy curve for the reaction. The FEP/US approach may also be used to obtain the free-energy functional of the isolated diabatic states. For example, the diabatic free energy Δg_1 of the reactant state can be calculated as

$$\Delta g_1(x') = \Delta G_m - \beta^{-1}\ln\langle\delta(x - x')\exp[-\beta(\epsilon_1(x) - \epsilon_m(x))]\rangle_{\epsilon_m} \quad (5)$$

The diabatic free-energy profiles of the reactant and product states represent the microscopic equivalent of the Marcus' parabolas.[30]

To parametrize the EVB surface we started by fitting the gas-phase EVB surface to an ab initio surface represented by 26 points covering the reactant and transition-state region (see Table 1). These energy points were originally calculated with a Poisson−Boltzmann (PB) solver and a dielectric constant (ϵ = 4) as a simplified model of the environment. Ideally, this fitting should have been done with ab initio vacuum potentials, but since the charge transfer is small in this system, these potentials are very similar, and the PB energy points can be used as a model for the vacuum calculation. The calculation of each point, defined by fixing the C−O distance and the C−H or O−H distance, was performed using the hybrid density functional B3LYP method in its spin-unrestricted form.[31−33] The geometry of the model complex was first optimized with a double-ζ basis set, and then the energy was recalculated for this geometry with a basis set of triple-ζ quality and a single set of polarization function on each atom, lacv3p**. For iron, a nonrelativistic effective core potential (ECP) was used.[34] All ab inito calculations were carried out using the Jaguar program.[35] Since the protein+solvent environment is treated considerably better in the EVB method, we have further refined the EVB surface to reproduce the experimental $k^{\mathrm{H}}_{\mathrm{cat}}$ at 300 K. This was done, however, without using any information about the isotope effect or the temperature dependence of k_{cat}.

Table 1. B3LYP DFT Energy Points for Representing the Potential Energy Surface for the Lipoxygenase Reaction

C–O	C–H	O–H	Δ*E* (kcal/mol)	C–O	C–H	O–H	Δ*E* (kcal/mol)
3.80	1.10	3.92	0.00	2.60	1.10	2.35	5.68
	2.86	0.97	−11.49		1.20	1.42	13.26
3.00	1.10	2.97	0.23		1.30	1.31	15.39
	1.50	1.50	24.88		1.40	1.20	11.21
	2.03	0.98	−10.10		1.50	1.10	4.23
2.80	1.10	2.67	2.01		1.64	0.98	−3.28
	1.20	1.77	7.42	2.50	1.09	2.24	8.54
	1.30	1.53	15.33		1.20	1.32	16.38
	1.40	1.40	20.01		1.30	1.20	14.55
	1.50	1.30	15.54		1.40	1.10	8.45
	1.84	0.98	1.63		1.50	1.00	2.31
				2.40	1.09	2.17	12.71
					1.20	1.21	19.06
					1.30	1.11	14.19
					1.40	1.02	8.97

The classical activation free energy was obtained with regular EVB/umbrella sampling procedures. That is, all simulations have been performed similar to standard MOLARIS all-atom simulation.[26,36] The system is spherical and divided into four regions: Region 1 is the EVB region that contains the essential interaction parameters for the reaction (in this case the bond Morse potentials, harmonic angle potentials, point charges, and van der Waals parameters associated with the CH_2 atoms of the lipid, the OH molecule, and the Fe atom and its directly ligating atoms). Region 2 contains protein and solvent atoms up to an 18 Å radius and is represented with the standard ENZYMIX force field,[36] where the solvent molecules are subjected to the surface-constrained all-atom solvent (SCAAS) boundary[37] and the local reaction field (LRF) model.[38] The remaining protein atoms are kept fixed in their initial position during the simulation. This system is finally embedded in a 2 Å shell of Langevin dipoles and a dielectric continuum to simulate the bulk solvation. The reaction is then driven by changing the force-field parameters from the reactant state to the radical intermediate in 21 steps. Each of these steps has been simulated for 40 ps. Finally, the obtained 84,000 energy points have been used to obtain the classical reaction profile in Figure 1.

II.2. QCP Simulations. With the analytical EVB surface of the reacting system and its surrounding protein+water system, our task is to obtain the quantum correction to the classical activation free energy. To do this, we use the quantum classical path (QCP) method developed in previous studies of NQM effects in chemical reactions in solution and proteins.[6,8]

(27) Hwang, J. K.; King, G.; S., C.; Warshel, A. *J. Am. Chem. Soc.* **1988**, *110*, 5297−5311.
(28) Warshel, A.; Chu, Z. T.; Hwang, J. K. *Chem. Phys.* **1991**, *158*, 303−314.
(29) Warshel, A. *Computer Modeling of Chemical Reactions in Enzymes and Solutions*, 1997 ed.; John Wiley & Sons: New York, 1997.
(30) Marcus, R. A. *Annu. Rev. Phys. Chem.* **1964**, *15*, 155.
(31) Becke, A. D. *Phys. Rev. A* **1988**, *38*, 3098−3100.
(32) Becke, A. D. *J. Chem. Phys.* **1993**, *98*, 1372−1377.
(33) Becke, A. D. *J. Chem. Phys.* **1993**, *98*, 5648−5652.
(34) Hay, P. J.; Wadt, W. R. *J. Chem. Phys.* **1985**, *82*, 299−310.
(35) *Jaguar*, 4.0 ed.; Schrodinger Inc.: Portland, OR, 1991−2000.
(36) Lee, F. S.; Chu, Z. T.; Warshel, A. *J. Comput. Chem.* **1993**, *14*, 161−185.
(37) King, G.; Warshel, A. *J. Chem. Phys.* **1989**, *91*, 3647−3661.
(38) Lee, F. S.; Warshel, A. *J. Chem. Phys.* **1992**, *97*, 3100−3107.

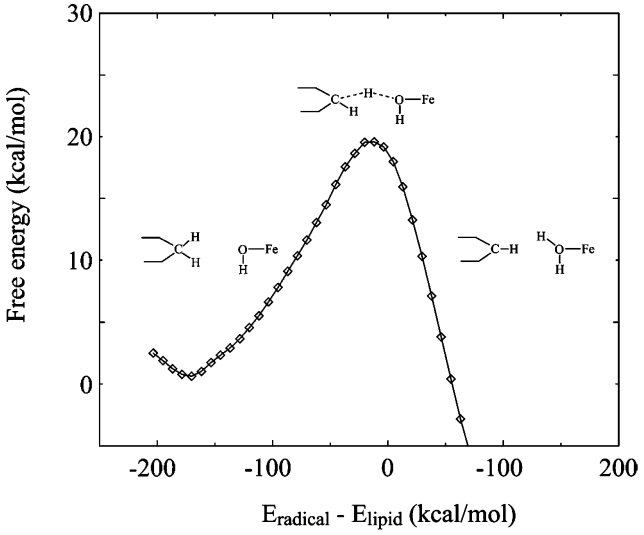

Figure 1. The classical free-energy barrier for transferring the hydrogen atom from the lipid substrate to form the radical intermediate.

The QCP approach, which is a version of the path integral approach[23,24] expresses the nuclear quantum mechanical rate constant as

$$k_{qm} = F_{qm}\{k_B T/h\}\exp(-\beta \Delta g^{\ddagger}_{qm}) \quad (6)$$

where F_{qm}, k_B, T, h, and β are, respectively, the transmission factor, Boltzmann's constant, the temperature, Planck's constant, and $\beta = 1/k_B T$. The quantum mechanical activation barrier, $\Delta g^{\ddagger}_{qm}$, includes almost all the nuclear quantum mechanical effects, whereas only small effects come from the pre-exponential transmission factor in the case of systems with a significant activation barrier.[7,39] For convenience (and numerical stability) we therefore divide the reaction free energy into classical and quantum mechanical parts according to

$$\Delta g^{\ddagger}_{qm}(T) = \Delta H^{\ddagger}_{cl} - T\Delta S^{\ddagger}_{cl} + \Delta\Delta g^{\ddagger}_{cl\to qm}(T) \quad (7)$$

where the quantum mechanical correction can further be divided into a temperature-independent and temperature-dependent term

$$\Delta\Delta g^{\ddagger}_{cl\to qm}(T) = \Delta\Delta H^{\ddagger}_{cl\to qm} - T\Delta\Delta S^{\ddagger}_{cl\to qm}(T) \quad (8)$$

The quantum mechanical free-energy barrier, $\Delta g^{\ddagger}_{qm}$, can be evaluated by Feynman's path integral formulation,[40] where each classical coordinate is replaced by a ring of quasiparticles that are subjected to the effective "quantum mechanical" potential

$$U_{qm} = \sum_{k=1}^{p} \frac{1}{2p} M\Omega^2 \Delta x_k^2 + \frac{1}{p} U(x_k) \quad (9)$$

Here, $\Delta x_k = x_{k+1} - x_k$ (where $x_{p+1} = x_1$), $\Omega = p/\hbar\beta$, M is its mass, and U is the actual potential used in the classical simulation. The total quantum mechanical partition function can then be obtained by running classical trajectories of the quasiparticles with the potential U_{qm}. The probability of being at the transition state is this way approximated by a probability distribution of the center of mass of the quasiparticles (the centroid) rather than the classical single point.

The use of quasiparticles is a computational device whose use in explaining quantum effects is less straightforward than many qualitative (and less reliable) models. Nevertheless, we provide in Figure 2 a qualitative rationalization for the fact that the path integral approach is able to evaluate quantum mechanical effects. The figure compares the classical and quantized description, red and green lines respectively, of a particle for a simple schematic one-dimensional potential. As illustrated by the figure, a classical particle (red balls) with a total energy $E < U^{\ddagger}$ cannot pass from the left to the right side of the potential since its energy is lower than the value of the potential at the transition state, $x^{\ddagger}$. On the other hand, a quantum mechanical particle (represented by the ring of green balls) can penetrate or "tunnel" through the barrier since each of the quasiparticles only experiences the potential $U(x_k)/p$ rather than $U(x_k)$; note, however, that when p increases there is on average less energy per particle. This results in a nonzero probability to be at the transition state in the quantum description even though the total energy is lower than the transition-state energy. The only reason that tunneling does not occur so readily is the restoring force of the $M\Omega^2\Delta x^2_k/2p$ term that "connects" the quasiparticles close to each other at high temperature (small β), and similarly, when M is large, the system behaves classically. However, at low temperature and when M is small, the quasiparticles can spread and some of them can penetrate the barrier. The quantum mechanical probability that the system will reach $x^{\ddagger}$ is given by the chance that the center of mass of the quasiparticle ring will be at this point. Similarly, the centroid path integral approach reproduces the quantum mechanical effects of the zero-point energy. That is, in the classical limit at low temperature the particle will relax to x_0. On the other hand, in the quantum limit the systems will always have nonzero potential energy when the centroid position is at x_0 since some of the quasiparticles will be at $x_k \neq x_0$. Thus, at low temperature the quasiparticles can be at points whose potential energy are larger than $U(x_0)$ and will have larger average potential energy than the corresponding classical particle. These effects reflect the zero-point energy.

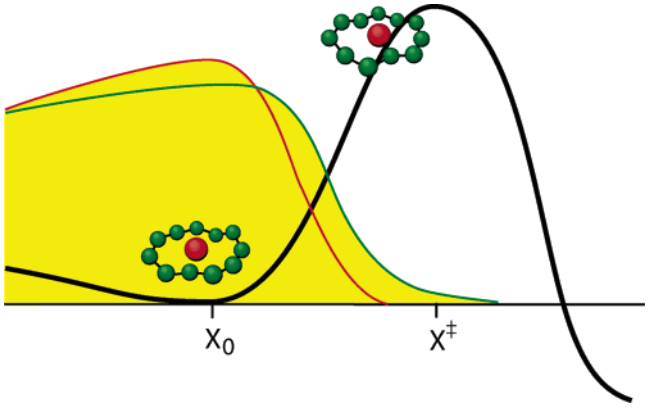

Figure 2. Showing a schematic behavior of the classical and quantum mechanical description of a proton-transfer reaction. In the QCP quantum mechanical description, the nuclear wave function, and thereby the nuclear distribution, is given by an ensemble of quasiparticles (here depicted as a ring of green particles), whereas in the classical picture it is given by a point particle (here depicted as a red particle). Similarly, the overall probability distribution is given for the classical and quantum mechanical description by the red and green line, respectively. Close to the reactant geometry, x_0, the quasiparticles can be at positions higher in energy than the point particle, which reflects the zero-point energy. In contrast, at an energy $E < U(x^{\ddagger})$ the classical point particle cannot reach the transition-state region, whereas some of the quasiparticles in the quantum mechanical description can. This gives a nonzero probability to penetrate the reaction barrier and results in nuclear tunneling.

Actual calculations of centroid probabilities in condensed phase reactions are very challenging and may have major problems with convergence. The QCP approach offers an effective and rather simple way for evaluating this probability without changing the simulation program significantly. This is done by propagating classical trajectories on the classical potential energy surface of the reacting system and using the positions of the atom of the system to generate the centroid position for the quantum mechanical partition function. This treatment is based on the finding that the quantum mechanical partition function can be expressed as[15,19]

(39) Warshel, A.; Parson, W. W. *Q. Rev. Biophys.* **2001**, *34*, 563−679.
(40) Feynman, R. *Statistical Mechanics*; Benjamin: New York, 1972.

$$Z_q(\bar{x}) = Z_{cl}(\bar{x})\langle\langle \exp\{-(\beta/p)\sum_k U(x_k) - U(\bar{x})\}\rangle_{fp}\rangle_U \quad (10)$$

where $\bar{x}$ is the centroid position, $\langle ... \rangle_{fp}$ designates an average over the free particle quantum mechanical distribution obtained with the implicit constraint that $\bar{x}$ coincides with the current position of the corresponding classical particle, and $\langle ... \rangle_U$ designates an average over the classical potential U. Using eq 10, we can obtain the quantum mechanical free-energy surface by evaluating the corresponding probability by the same combined free-energy perturbation umbrella sampling approach of eq 4. Now we use the double average of eq 10 rather than an average over a regular classical potential. At any rate, the main point of the QCP is that the quantum mechanical free-energy function can be evaluated by a centroid approach that is constrained to move on the classical potential. This provides stable and relatively fast converging results that have been shown to be quite accurate in studies of well-defined test potentials (where the exact quantum mechanical results are known[8]).

This work uses, as an initial geometry, the lipoxygenase pdb entry 1YGE in the Brookhaven protein data bank, which is known to 1.4 Å resolution.[41] Since, to the best of our knowledge, no structure has been solved with a substrate, we have manually docked in a substrate model ($CH_2CHCH_2CHCH_2$) and equilibrated the system thoroughly to avoid short contacts and to better position it. Even though this model is considerably smaller than the natural fatty acid, it still has all the important attributes of the substrate and, thus, should not give any significant additional errors.

To obtain the NQM effects we run classical trajectories of the quasiparticles on the "quantum mechanical" potential given by eq 9. For these trajectories, we have used between 10 and 20 particles (a quantity less than 10 particles seems to give unstable results; for the results presented in this study, 18 particles are used). Also, since any reliable protein investigation should average the relevant energies over protein configurations, the energy of the quasiparticle trajectory has been averaged for every 0.5 fs of a 10 ps protein simulation. In the end, the $\Delta\Delta g^{\ddagger}_{cl\rightarrow qm}(T)$ term is averaged over 20,000 protein and quasiparticle configurations. To compensate for the comparatively short simulation over the protein configurations (it turns out to be very time-consuming to average both over protein and quasiparticle configurations with an 18-particle system), the system was first equilibrated thoroughly for 500 ps.

II.3. Qualitative Vibronic Approach. As was stated in the Introduction, our system cannot be described by using the diabatic limit. Nevertheless, it may be useful to discuss some features of the corresponding rate constant. That is, in the case of weakly coupled reactant and product state, i.e., small H_{12}, one can express the rate constant by (see, e.g., refs 15,16)

$$k_{12} = \frac{\sum_{mm'} k_{1m,2m'} \exp\left\{-\sum_r \hbar\omega_r(m_r + 1/2)/k_BT\right\}}{\sum_m \exp\left\{\sum_r \hbar\omega_r(m_r + 1/2)/k_BT\right\}}$$

$$k_{1m,2m'} = |H_{12}S_{mm'}/\hbar|^2(\pi\hbar^2/k_BT\lambda_{cl})^{1/2}\exp[-\Delta g^{\ddagger}_{mm'}/k_BT] \quad (11)$$

where λ_{cl} is the classical solvent reorganization energy, which reflects the classical modes, and $S_{mm'}$ is the Franck−Condon factor for the transition between the m and m' vibronic levels (which involve excitation of the vibrations w_r) of the reactant and product states, respectively. The activation free energy, $\Delta g_{qm}^{\ddagger}$, can be approximated by

$$\Delta g^{\ddagger}_{mm'} = [\Delta G^0 - \sum_r \hbar\omega_r(m'_r - m_r) + \lambda_{cl}]^2/4\lambda_{cl} \quad (12)$$

The above equation is valid in the high-temperature limit and an extension to the low-temperature limit is readily available (see ref 16). It is also important to note that eq 12 should include ΔG^0 rather than the previously assumed ΔE^0 as established in references.[16,42] At any rate, since we cannot trust eq 11 when H_{12} is large, we will here only use it to qualitatively discuss the dependence of the NQM effects on λ_{cl}.

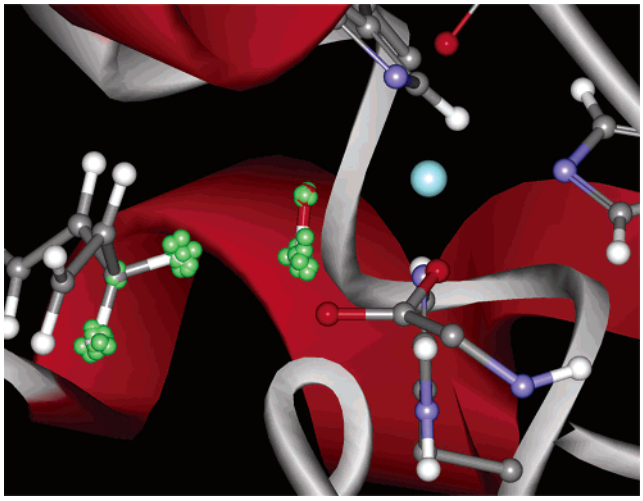

Figure 3. Showing a snapshot of the quasiparticles (depicted in green) during the simulation. The quasiparticles are used to represent the probability density of the reacting atoms in lipoxygenase. This representation enables the atoms to be in classically forbidden configurations and, thus, tunnel through the barrier. It can further be seen that the distribution of quasiparticles are more spread out for lighter particles (i.e., the hydrogen atoms) than for the heavier (e.g., the carbon and oxygen atoms), which results in an increased tunneling.

III. Results and Discussion

Previous vacuum ab initio calculations[5,14] of the potential energy surface of the hydrogen atom transfer in a minimal model for lipoxygenase have obtained activation barriers in the range of 12−34 kcal/mol, depending on the distance between the donor and acceptor atoms, basis set, and model size. The challenge, however, is to add the effect of the protein to the calculated surfaces of the subsystem and then to evaluate the rate constant with the nuclear quantum effects. This should reproduce the observed isotope effect and temperature dependence of the rate constant.

To address the above challenges, we started by calibrating the gas-phase EVB potential energy surface using a B3LYP DFT profile according to the procedure described in section II.1. The resulting potential was then used in the QCP simulations. A snapshot from our simulation is shown in Figure 3. As mentioned in section II.2, the quasiparticles (here depicted in green) are used to represent the probability distribution of the reacting atoms. This way, atoms are able to partially be in regions that are energetically unavailable for a classical non-tunneling representation. More specifically for lipoxygenase, the hydrogen atom that is being transferred from the lipid has a larger probability of being closer to the acceptor group (the OH ligand bound to the Fe ion) and, thus, tunnel through the reaction barrier. It can also be seen that the distribution of quasiparticles are more spread out for lighter particles (i.e., the hydrogen atoms) than for the heavier (e.g., the carbon and oxygen atoms), which increases their tunneling. At any rate, collecting the

(41) Minor, W.; Steczko, J.; Stec, B.; Otwinowski, Z.; Bolin, J. T.; Walter, R.; Axelrod, B. *Biochemistry* **1996**, *35*, 10687−10701.
(42) Warshel, A. *J. Phys. Chem.* **1982**, *86*, 2218−2224.

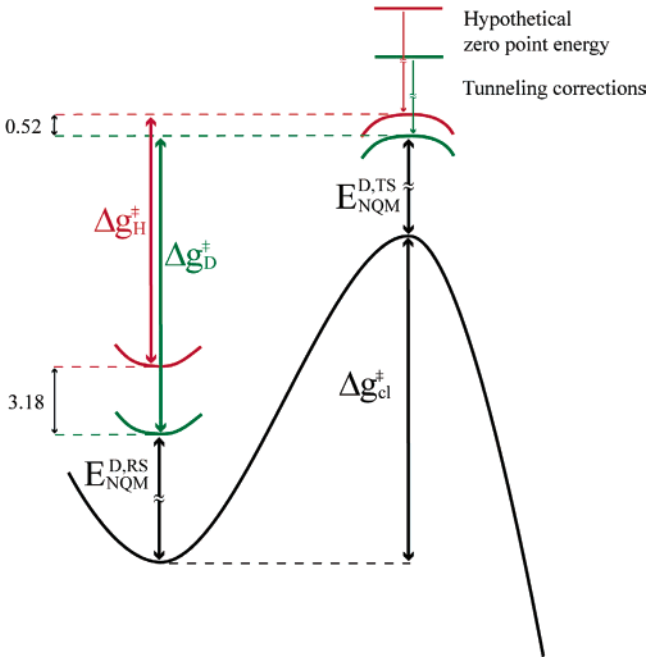

Figure 4. Showing the quantum mechanical corrections to the classical surface at the reactant state (RS) and transition state (TS). The nuclear quantum mechanical contributions (the zero-point energy [ZPE] and nuclear tunneling) are calculated by the QCP approach for the reactant and transition state (E_{NQM}^{RS} and E_{NQM}^{TS}). At the reactant-state geometry this contribution is dominated by the zero-point energy, whereas at the transition state, the zero-point energy is reduced by nuclear tunneling. Both these correction terms are larger for the lighter hydrogen atom, as compared to the deuterium, and results in a lower quantum mechanical reaction barrier for the hydrogen transfer ($\Delta g^{\ddagger}_{H}$ versus $\Delta g^{\ddagger}_{D}$). The figure helps to emphasize that the quantum mechanical free energy at the TS reflects the competition between comparatively large positive ZPE and an opposing negative tunneling contribution. Since the QCP method does not separate the ZPE and tunneling contributions, we only provide a hypothetical estimate of the ZPE at the TS.

statistics from the QCP simulation according to eq 10 in the framework of the umbrella sampling/FEP formulation of section II.1 provided the quantum correction to the classical free-energy profile. The quantum corrections for the ground-state and transition-state regions at 300 K, are shown in Figure 4. Close to the reactant geometry, x_0, the E_{NQM} contains almost entirely the zero-point energy, whereas at the transition state, $x^{\ddagger}$, the quantum mechanical correction term contains large contributions from both zero-point energy and nuclear tunneling. These contributions cannot readily be separated in the QCP approach.

Although it is quite easy to adjust the EVB parameters so that the observed activation barrier for H transfer at a specific temperature is reproduced, it is much more challenging to reproduce the observed KIE without adjusting any parameter, and it is very challenging to reproduce the temperature dependence of the rate constant. To address these challenges we introduced the following two-step strategy. First we evaluated the classical activation barrier (by the classical EVB surface and the umbrella sampling/FEP approach) at three temperatures (270, 300 and 333 K) to obtain the classical activation enthalpy and entropy ($\Delta H^{\ddagger}_{cl}$ and $\Delta S^{\ddagger}_{cl}$, respectively). This expansion, which corresponds to eq 7 with $\Delta\Delta g^{\ddagger}_{cl\rightarrow qm}(T) = 0$, gives $\Delta\Delta H^{\ddagger}_{cl} = 16$ kcal/mol and $-T\Delta\Delta S^{\ddagger}_{cl} = 4$ kcal/mol at $T = 300$ K. Next, we evaluated the QCP quantum correction, $\Delta\Delta g^{\ddagger}_{cl\rightarrow qm}(T)$, in the reactant and transition state regions for the same three temperatures. This type of analysis was found in our computer experiment to be the most robust analysis. Using this procedure,

Table 2. Calculated and Observed Kinetic Parameters for Lipoxygenase Obtained in This Study[a]

temp (K)	k^{H}_{cat} (s^{-1})	k^{D}_{cat} (s^{-1})	KIE	$\Delta g^{\ddagger}_{H}$ (kcal/mol)	$\Delta g^{\ddagger}_{D}$ (kcal/mol)	$\Delta g^{\ddagger}_{cl}$ (kcal/mol)
270	322 (189)	1.0 (2.0)	380	12.70 (13.02)	15.89 (15.47)	19.59
300	507 (297)	6.0 (3.7)	86	13.84 (14.16)	16.50 (16.79)	19.99
333	541 (392)	18 (5.7)	60	15.27 (15.46)	17.98 (18.67)	20.43

[a] We provide in brackets relevant experimental results estimated using the kinetic parameters of ref 1.

we can average the classical free energy extensively to get an accurate free-energy profile and a division into enthalpy and entropy. This would virtually be impossible to simulate at the same time as running trajectories over quasiparticle configurations since the calculation time increases linearly with the number of particles. The simulation of the nuclear quantum mechanical correction, however, is less sensitive to sampling over protein configurations, provided that the same reference potential is used for both the hydrogen and deuterium form of the reactants. It is also easier to obtain converged values for the simulation of the temperature dependence of these corrections since the temperature dependence is explicitly included in the potential, U_{qm} (Ω in eq 9) rather than implicitly as in the case of the classical free energy.

The results of our analyses are summarized in Table 2 and Figure 5. Table 2 provides a summary of the quantum mechanical rate constants, KIE and the corresponding $\Delta g^{\ddagger}_{cl}$ and $\Delta g^{\ddagger}_{qm}$ for the different temperatures. The Arrhenius plot, Figure 5, depicts the relationship between log k and $1/T$ for three values of $\Delta H^{\ddagger}_{cl}$ (15, 16, and 17 kcal/mol, green, red, and blue, respectively), which reflect the error range in our EVB refinement procedure. All these are almost parallel to the experimental (black) line. The figure also includes, for comparison, classical (dashed) lines that correspond to the same $\Delta H^{\ddagger}_{cl}$ and $\Delta S^{\ddagger}_{cl}$, but without NQM effects. Clearly, the $\Delta\Delta g^{\ddagger}_{cl\rightarrow qm}$ term and its decomposition depend also on simulation conditions; however, the uncertainties are small enough to make the three colored lines in Figure 5 representative of what we obtained.

Interestingly, the classical activation free energy is relatively large for all these lines, giving $\Delta G^{\ddagger}_{cl}(300) \approx 20$ kcal/mol. The rather large quantum correction ($\sim$6 kcal/mol), however, lowers the reaction free energy considerably, and we obtain $\Delta g^{\ddagger}_{qm}(300) \approx 14$ kcal/mol, which corresponds to $k_{cat,qm} \approx 500\ s^{-1}$ and is very close to the observed $k_{cat,obs} = 300\ s^{-1}$. It seems that the three calculated lines reproduce the experiment well. It is also very significant to note, see Table 2, that we reproduced all the observed activation free energies at all temperatures within $\sim$0.5 kcal/mol.

As is clear from the large calculated and observed isotope effect and the small slope of the Arrhenius plot, SLO-1 exhibits a very large NQM effect, which is consistent with an exceptionally large tunneling contribution.[1] However, since the centroid path integral approach gives the total NQM effect, it is hard to determine what the actual contributions from zero-point energy and tunneling are. At any rate, our main point is to evaluate the overall NQM effect and to demonstrate that the QCP approach can reproduce such a large effect.

It is interesting to consider the calculated enthalpic and entropic contributions to $\Delta\Delta g^{\ddagger}_{cl\rightarrow qm}$. The calculations of $\Delta\Delta H^{\ddagger}_{qm}$ and $\Delta\Delta S^{\ddagger}_{qm}$ were found to be -14.3 kcal/mol and -27.5 cal/mol K, respectively, for the H transfer reaction. This gives

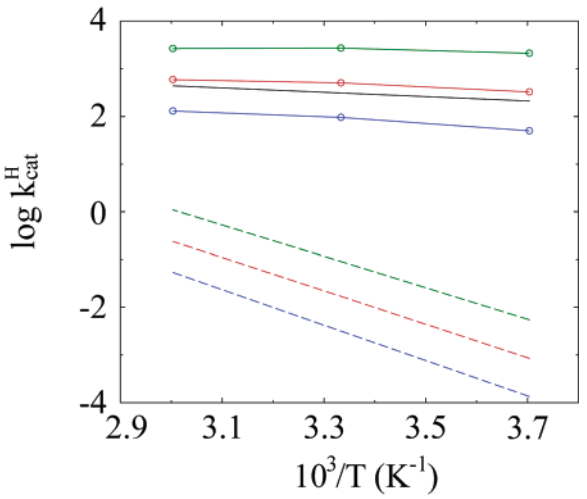

Figure 5. Arrhenius plot. The figure depicts the experimental results (solid black) and the corresponding theoretical results obtained for lipoxygenase; $\Delta H^{\ddagger}_{cl} = 15$ (red), 16 (green), and 17 kcal/mol (blue), and $-T\Delta S^{\ddagger}_{cl} = 4$ kcal/mol. The dashed lines show the barrier with the same classical free-energy contributions, $\Delta H^{\ddagger}_{cl}$ and $\Delta S^{\ddagger}_{cl}$, but without the nuclear quantum mechanical correction, $\Delta\Delta g^{\ddagger}_{cl\rightarrow qm}$ in eq 7.

$\Delta H^{\ddagger}_{qm} \approx 1.7$ kcal/mol, which is in very good agreement with the experimentally observed E_a^H, ($E_a^H \approx 2.1$). For the D transfer reaction we obtain -9.2 kcal/mol and 20.0 cal/mol K^{-1}, which gives $\Delta H^{\ddagger}_{qm} \approx 6.8$ kcal/mol and is in less impressive agreement with the observed ($E_a^D \approx 3.0$). Apparently although our approach can evaluate the very large difference between the classical and quantum mechanical temperature dependence, we are not yet at the stage where we can reproduce the much more challenging temperature dependence of the kinetic isotope effect (reproducing simultaneously E_a^H and E_a^D). The fact that this is a much less stable quantity can be established by the experimental observation that the Ile553Ala mutation changes A_H/A_D by a factor of 150 (and $E_a^H - E_a^D$ by -3.1 kcal/mol) while leaving k_{cat} and the KIE almost unchanged.[1] This point will be further discussed below and in section IV. Again, we emphasize that we succeeded in reproducing the overall experimental $\Delta g^{\ddagger}$ to within 0.5 kcal/mol, so that the relatively large deviation in $\Delta H^{\ddagger}$ is compensated by the changes in $-T\Delta S^{\ddagger}$ and we obtain a small deviation in $\Delta g^{\ddagger}$.

In general, it is extremely challenging to obtain quantitative entropic and enthalpic contributions by computer simulations of protein,[43,44] and it is much simpler to get stable activation free energy due in part to the well-known enthalpy−entropy compensation effect.[43] Thus, it is reasonable to find that we can reproduce the overall NQM contribution to the activation free energy of eq 7 but may have difficulties providing the detailed decomposition to temperature-dependent and -independent terms. At this point, we also mention that we are not aware of any other simulation approach that can actually evaluate the temperature dependence of the quantum activation free energy in proteins. Here, we do not consider gas-phase studies of hydrogen transfer reaction that may perhaps reproduce the small observed temperature dependence of the isotope effect but cannot simulate the effect of the protein and thus cannot help in elucidating the possible role of the protein in enhancing NQM effects. It is also interesting to comment on the fact that our study reproduced the observed temperature dependence and the activation enthalpy of the H transfer reaction but does worse in reproducing the trend in the D transfer reaction. It is well-known that in the case of significant tunneling effects, the rate constant is temperature independent and then starts to be temperature dependent.[39,46] The transition between tunneling to the activated region reflects the properties of the medium, e.g. the reorganization energy and other factors that may be hard to simulate exactly (especially when there is a competition between the classical entropic effect, e.g. the $\Delta S^{\ddagger}_{cl}$ of eq 7, and the quantum corrections). The corresponding difficulty may be appreciated by realizing, for example, that it is extremely hard to obtain the freezing point of a protein by MD simulation. More importantly, the main point of this contribution is the ability to obtain stable results for the KIE and reasonable NQM effects. This ability should allow us to use the QCP method to explore the catalytic contribution of NQM effects (see section IV).

Although our main aim is the establishment of a reliable simulation approach that reproduces NQM contributions to activation free energies, it is of interest to examine why some enzymatic reactions show large NQM effects and large KIE, while others only show small effects. Here one can consider two issues, the nature of the intrinsic potential surface and the coupling to the protein environment.

To explore this, we performed several additional calculations. First we evaluated the NQM contributions for the reaction of the active-site cluster in water, the reference reaction referred to in section I. The calculation for 300 K gave the $\Delta g^{\ddagger}_{qm}$ values of 13.68 and 16.42 kcal/mol for H and D respectively, and a KIE close to 100 (however, since the simulation of the water system seems to give less stable results than the protein simulation, they are an average over several different runs and, unarguably, less accurate than the precision indicates). At any rate, these values are quite similar to the corresponding values in the enzyme (13.84 and 16.50 kcal/mol and 86 for $(\Delta g^{\ddagger}_{qm})_H$, $(\Delta g^{\ddagger}_{qm})_D$ and KIE, respectively). The significance of this finding will be discussed below.

In the second set of calculations, we have evaluated the total reorganization energy, λ, and its inner- and outer-sphere components according to

$$\lambda = \lambda_{qm}^{\ in} + \lambda_{cl}^{\ in} + \lambda_{cl}^{\ out} \qquad (13)$$

where λ_{qm} is the quantum mechanical contribution of λ (which is described by the corresponding Franck−Condon frequencies) and λ_{cl} is the classical contribution of the reorganization energy. The classical reorganization energy is further divided into inner- and outer-sphere contributions, which is denoted by the superscript "in" and "out". However, it is important to realize that the total reorganization energy is evaluated rigorously by our classical microscopic approach[45] with the diabatic EVB free-energy surfaces (e.g. the Δg_1 of eq 5). The total classical λ can then be decomposed into the different contributions of eq 13 by the dispersed polaron treatment (see ref 50) where the origin shifts and frequencies of the modes that are treated quantum mechanically in eq 12 determine λ_{qm}^{in}. It is also important to note that the above reorganization energies are evaluated by

(43) Levy, R. M.; Gallicchio, E. *Ann. Rev. Phys. Chem.* **1998**, *49*, 531−567.
(44) Villà, J.; Strajbl, M.; Glennon, T. M.; Sham, Y. Y.; Chu, Z. T.; Warshel, A. *Proc. Natl. Acad. Sci. U.S.A.* **2000**, *97*, 11899−11904.
(45) King, G.; Warshel, A. *J. Chem. Phys.* **1990**, *93*, 8682−8692.
(46) DeVault, D. *Q. Rev. Biophys.* **1980**, *13*, 387−564.

classical simulations and not by the QCP treatment, which is not based on eq 12 but rather considers the dynamics of the system by a much more rigorous quantum treatment.

The values of the inner-sphere reorganization energy are not so relevant here since the largest component comes from the stretching and bending coordinates, which are treated quantum mechanically (corresponding to λ_{qm}^{in} in eq 13). It also reflects the effect of the donor and acceptor distance on the contribution from the stretching coordinate to the energy gap ($\epsilon_2 - \epsilon_1$). Furthermore, the intramolecular reorganization energy is strongly correlated with H_{12}, a point that is rarely realized in the field (as discussed in ref 16, a smaller H_{12} and smaller λ will give the same adiabatic barrier). The outer-sphere contribution to the reorganization energy, on the other hand, is a meaningful parameter that can fairly readily be obtained from MD simulations, as is well-known in the field of ET; see, for example, ref 39. Thus, the main point of the present analysis is the evaluation of the outer-sphere reorganization energy (λ_{cl}^{out}). The outer-sphere reorganization energy was evaluated by the linear response approximation[47] that allows us to decompose the reorganization energy into additive contributions that are evaluated according to

$$\lambda^{\alpha} = 1/2[\langle \epsilon_2{}^{\alpha} - \epsilon_1{}^{\alpha} \rangle_1 - \langle \epsilon_2{}^{\alpha} - \epsilon_1{}^{\alpha} \rangle_2] \qquad (14)$$

Here, λ^{α} is the αth contribution to the reorganization energy (e.g., the electrostatic contribution) and $\langle ... \rangle_i$ designates a MD average over state *i*. Our calculation found an extremely small λ_{cl}^{out}, i.e., $\sim 2.5 \pm 1$ kcal/mol for both the solvent and protein reactions. This is clearly a much smaller value than the 20−30 kcal/mol that has been estimated from phenomenological fitting to eq 11 (e.g., ref 1). Of course, λ_{cl} also includes intramolecular modes of the reacting system (inner sphere) that are not included in the quantum mechanical representation of eq 12. The corresponding values can be evaluated rigorously by the dispersed polaron treatment. This is out of the scope of this work since the use of eq 12 is qualitative. However, it is clear that the modes which correspond to the donor−acceptor distance contribute significantly to λ_{cl}^{in}.

In general, we are aware of other cases where phenomenologically fitted reorganization energies did not correspond to the value obtained by a proper microscopic treatment (e.g., see ref 22). At any rate, the most important finding of this analysis is the fact that the protein or solvent reorganization energy is only ~3 kcal/mol, which is considerably smaller than the typical value of ~20 kcal/mol obtained for proton, electron, and other charge transfer reactions (e.g., refs 6, 10, and 48).

Since the protein, or solvent, modes have very small effect on our reacting system (the solute) as can be judged from the very small outer-sphere reorganization energy, it is clear that the NQM effects primarily reflect the properties of the reacting system. Thus, the large KIE seem to reflect the fact that the "solute" potential energy surface is rather narrow. In fact, our very early study of another hydrogen transfer reaction[49] also provided a large KIE.

It is also useful to point out that λ_{cl}^{out} is small, not because the protein is rigid as was previously suggested,[15] but because the reaction is associated with a minimal charge transfer and, thus, a small response by the protein environment (the possible effect of λ_{cl}^{out} on the temperature dependence of the KIE will be considered in the next section).

IV. Concluding Remarks

Examination of the role of NQM effects in enzyme catalysis is a problem of significant current interest (e.g., refs 1, 3, 6). To explore this issue in a unique way it is very advantageous to augment the available experimental approaches by reliable simulation methods capable of reproducing the relevant NQM corrections to the activation free energy and to allow one to analyze the protein contributions to this effect. To validate such approaches it is useful to demonstrate the performance of the given simulation method by reproducing large NQM effects and large KIE. This work used the QCP method in simulating the very large KIE and large NQM effect of lipoxygenase. We have demonstrated the robustness of the method in evaluating the NQM effect and obtained reasonable results in the extreme challenging task of evaluating the temperature dependence of the rate constant for the H atom transfer reaction but obtained less encouraging results in simulating the temperature dependence of the rate constant for the D transfer reaction. The difficulties of reproducing the temperature dependence of the rate constant reflect a well-known difficulty in reproducing temperature dependence of free energies by microscopic simulation.[43,44] It also seems to reflect an actual physical instability demonstrated by the effect of the Ile553Ala mutation that changes A_H/A_D by a factor of ~150 while leaving k_{cat} (and therefore $\Delta\Delta g^{\ddagger}$) unchanged.[1] Thus, despite the difficulties of obtaining the temperature dependence of the KIE, we have demonstrated that the QCP approach satisfies our requirement of obtaining a robust way to evaluate NQM contributions to activation free energies (this is established in Table 2).

It is interesting to discuss the decomposition of $\Delta g^{\ddagger}$ into effective enthalpic and entropic contributions. We find that the rather large classical activation enthalpy ($\Delta H^{\ddagger} \approx 16$ kcal/mol) is reduced drastically by a negative contribution from the $\Delta\Delta H^{\ddagger}_{cl\rightarrow qm}$ term in eq 8. The entropic contribution, on the other hand, increases $\Delta g^{\ddagger}_{qm}$ with both its classical and quantum mechanical contributions. Thus, the total $\Delta g^{\ddagger}$ reflect a major compensation between enthalpic and entropic contributions. This compensation is the reason (despite the difficulties of evaluating the exact $\Delta\Delta S^{\ddagger}_{qm}$ and $\Delta\Delta H^{\ddagger}_{qm}$ for both the H and D transfer reactions) we obtain very reasonable overall $\Delta\Delta g^{\ddagger}_{qm}$ for both H and D.

The overall trend of the transition of the rate constant from temperature-independent to temperature-dependent range is extremely well-known in the electron transfer (ET) community (see, e.g., ref 46). Such trends were reproduced previously in simulating ET reactions in the inverted region.[50] In the case of proton and hydrogen atom transfer reactions the challenge of reproducing the temperature dependence is larger since the coupling of the solute and solvent coordinates is more complex and the reaction is usually inherently adiabatic (this makes the use of simple analytical rate expressions problematic). In general, the temperature dependence of the NQM effect can be

(47) Muegge, I.; Qi, P. X.; Wand, A. J.; Chu, Z. T.; Warshel, A. *J. Phys. Chem. B* **1997**, *101*, 825−836.
(48) Bjerrum, M. J.; Casimiro, D. R.; Chang, I. J.; Dibilio, A. J.; Gray, H. B.; Hill, M. G.; Langen, R.; Mines, G. A.; Skov, L. K.; Winkler, J. R.; Wuttke, D. S. *J. Bioenerg. Biomembr.* **1995**, *27*, 295−302.
(49) Warshel, A.; Bromberg, A. *J. Chem. Phys.* **1970**, *52*, 1262-.
(50) Warshel, A.; Chu, Z. T.; Parson, W. W. *Science* **1989**, *246*, 112−116.

due to coupling of the reaction coordinate with both the orthogonal solute and solvent coordinates. This may involve fluctuations of the classical modes and the corresponding difference between the potential energy of the reactant and product state and fluctuations in the donor−acceptor distance and, thereby in H_{12}. The increase in the fluctuations of classical modes is expressed in the vibronic approach in the reorganization energy, λ_{cl}. In general, if the reorganization energy is temperature-dependent we may reach a point where λ_{cl} is sufficiently large to move us from the tunneling region to the activated region. This is particularly true in the present case, which would correspond to the inverted region *if the diabatic limit was valid*. Assuming, however, that the general trend of eq 11 is qualitatively relevant, one would have expected k_D to become classical before k_H when λ_{cl} is increased by the temperature. However, in the present case, the contribution of the protein to λ is very small and unlikely to play any significant role in controlling the temperature dependence of the rate constant. Nevertheless, the contribution of the reacting fragments to the temperature dependence of λ_{cl} (i.e., λ_{cl}^{in}) might affect the temperature dependence of the rate constant. It is also possible that the interaction between the protein and the substrate changes λ_{cl}^{in} and thus affects the temperature of transition between the tunneling and activated ranges. Unfortunately, obtaining the exact transition temperature is very challenging and is clearly out of scope of the present work.

We also feel that the interest in evaluating the temperature dependence of the NQM effects is somewhat overrated as much as enzyme catalysis is concerned. Here the main issue is the difference between the activation free energies of the reactant in the enzyme and in solution. As is clear from Table 2, we can reproduce $\Delta g^{\ddagger}_H$ and $\Delta g^{\ddagger}_D$ in all the temperatures studied despite the difficulty in reproducing the observed temperature dependence of the KIE. One may consider the difference of ∼0.5 kcal/mol between the calculated and observed activation barrier as a significant problem (although the experimental error is around 0.3 kcal/mol). However, when the difference between the classical and quantum activation barrier is in the range of 0.5 kcal/mol, we anyhow do not have a significant NQM (in this case the NQM contributions to catalysis is also small). Thus, we feel that we have a reliable tool for studying the NQM contributions to catalysis.

The present work compared the NQM contribution to the activation free energy in both the enzyme and the gas-phase reactions and found the corresponding contributions to be similar. The same calculations were performed for the solution reaction in which we obtained a KIE of ∼100. This should be compared to the 86 obtained for the protein reaction. However, it seems that this value is more sensitive to proper sampling, and therefore more uncertain, for the water simulation than for the protein. At any rate, the NQM contribution to k_{cat} appeared to be very similar in the two systems, which indicates that the enzyme does not use NQM to catalyze its reaction in lipoxygenase.

Obviously, we are not yet at a stage where we can provide a general conclusion about the role of tunneling in enzyme catalysis. However, several points seem to emerge from this and earlier studies (e.g., ref 10). That is, it is in general hard for enzymes, which are quite flexible, to change the width of the solute potential energy surface in a drastic way and thereby modulate the NQM effects. The solvent contribution to the potential energy surface, and the reorganization energy, can be changed significantly in cases of charge transfer reactions,[51] but this does not seem to lead to large changes in the NQM effects.[6] Thus, although NQM effects can be quite large, they are usually similar in the enzyme and solution reactions.

Acknowledgment. This work was supported with computer time by University of Southern California High Performance Computing and Communication Center (HPCC), and financially by the Swedish research council, VR, and by NIH Grant GM-40283. We also thank J. Villa for initial discussions.

JA037233L

(51) Warshel, A. *Proc. Natl. Acad. Sci. U.S.A.* **1978**, *75*, 5250−5254.